Article

Robust induction of functional astrocytes using NGN2 expression in human pluripotent stem cells

Rapid astrocyte induction leveraging transient NGN2 expression

Human iPS cells → NGN2 / Dual SMADi → ~30 days → Astrocyte medium → human iPSC-derived astrocytes (hiAs)

Transcriptomic and functional comparison with human brain astrocytes

Vs.

Bulk RNAseq and scRNAseq
Calcium signalling
Inflammatory response

Transcriptomic comparison to other iPSC-derived astrocyte approaches

umap1 / umap2

Martin H. Berryer, Matthew Tegtmeyer, Loïc Binan, ..., Steven A. McCarroll, Ralda Nehme, Lindy E. Barrett

rnehme@broadinstitute.org (R.N.)
lbarrett@broadinstitute.org (L.E.B.)

Highlights

Rapid human astrocyte generation from iPSCs using transient NGN2 and astrocyte media

Assessment of inflammatory response, calcium dynamics and neuronal network support

High homogeneity at the single cell level and across independent cell lines

Key features of astrocyte dysfunction recapitulated in a trisomy 21 disease model
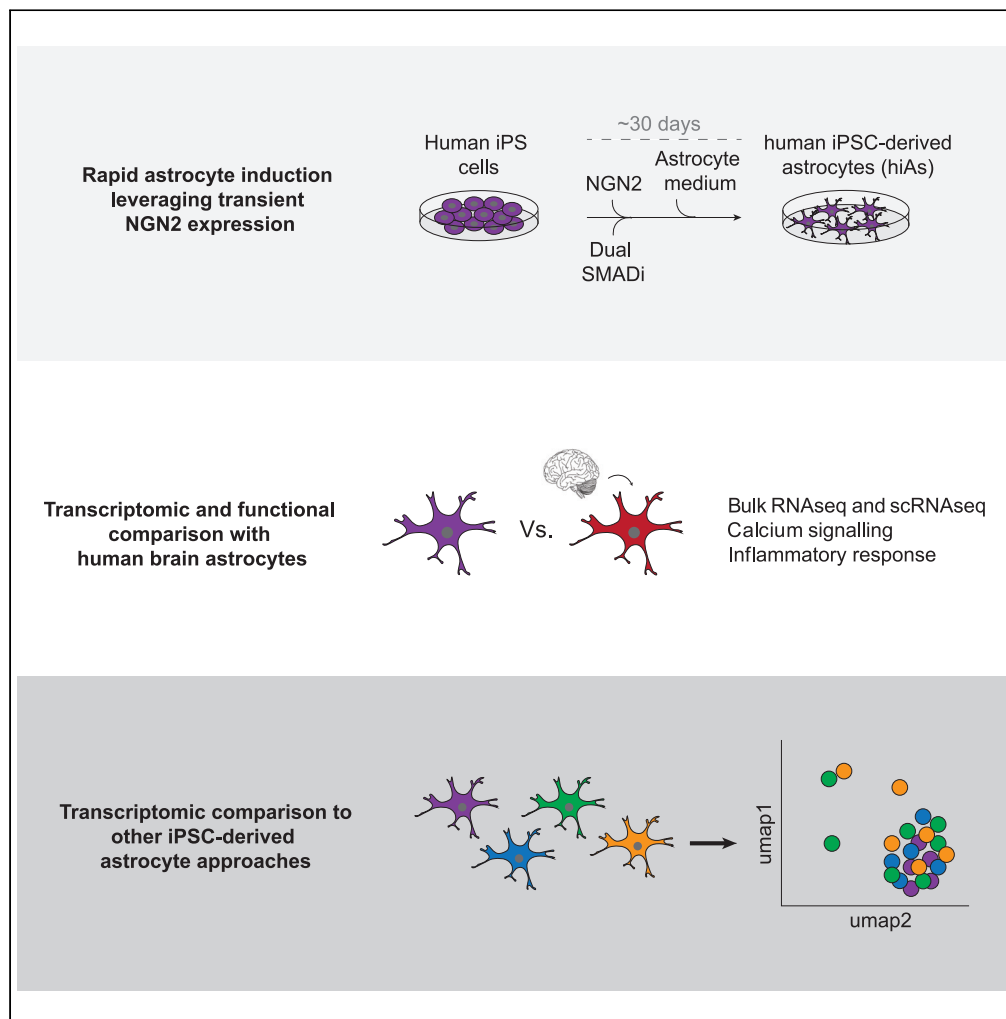
Article

Robust induction of functional astrocytes using NGN2 expression in human pluripotent stem cells

Martin H. Berryer,[1,2,7] Matthew Tegtmeyer,[1,2,3,7] Loïc Binan,[1,4] Vera Valakh,[1,4] Anna Nathanson,[1,2] Darina Trendafilova,[1,2] Ethan Crouse,[1,2] Jenny A. Klein,[1,2] Daniel Meyer,[1] Olli Pietiläinen,[1,5] Francesca Rapino,[2] Samouil L. Farhi,[1,4] Lee L. Rubin,[2] Steven A. McCarroll,[1,6] Ralda Nehme,[1,2,8,*] and Lindy E. Barrett[1,2,*]

SUMMARY

Emerging evidence of species divergent features of astrocytes coupled with the relative inaccessibility of human brain tissue underscore the utility of human pluripotent stem cell (hPSC) technologies for the generation and study of human astrocytes. However, existing approaches for hPSC-astrocyte generation are typically lengthy or require intermediate purification steps. Here, we establish a rapid and highly scalable method for generating functional human induced astrocytes (hiAs). These hiAs express canonical astrocyte markers, respond to pro-inflammatory stimuli, exhibit ATP-induced calcium transients and support neuronal network development. Moreover, single-cell transcriptomic analyses reveal the generation of highly reproducible cell populations across individual donors, mostly resembling human fetal astrocytes. Finally, hiAs generated from a trisomy 21 disease model identify expected alterations in cell-cell adhesion and synaptic signaling, supporting their utility for disease modeling applications. Thus, hiAs provide a valuable and practical resource for the study of basic human astrocyte function and dysfunction in disease.

INTRODUCTION

Astrocytes are the most abundant cell type in the human brain. They play crucial roles in regulating neuronal development, maturation, and synaptic connectivity.[1,2] Astrocyte dysfunction and defective astrocyte-neuron interactions have been implicated in a wide variety of disorders, including psychiatric, neurodevelopmental and neurodegenerative disorders.[1–3] Astrocytes also play an important role in regulating the cerebral microenvironment by interacting with endothelial and microglial cells that participate in the blood brain barrier[4–7] and communicating with oligodendrocytes via direct contact and secretion of cytokines and chemokines.[8–10]

Although brain cell types are largely thought to be conserved across species, an increasing number of studies have uncovered divergent molecular, structural, and functional features of glia. For example, transcriptional comparisons between human and rodent have revealed greater differences in glial gene expression signatures compared with neuronal-associated transcripts, suggesting that glial genes may be evolutionarily less conserved than neuronal genes.[11] Moreover, although mammalian astrocytes respond to glutamate and ATP by increasing intracellular calcium concentrations, human astrocytes support different calcium wave dynamics as compared with rodent astrocytes[12,13] which has the potential to affect subsequent release of glio-modulators. Pharmacological inhibition of the TGFβ pathway partially prevents the synaptogenic effect of murine astrocyte-conditioned media on cortical neurons but abolishes the effect of human astrocyte-conditioned media, suggesting that human astrocytes may rely more heavily on TGFβ signaling than their rodent counterparts.[14] Human astrocytes also display larger cellular diameters with more elaborated and compartmented processes compared with rodent astrocytes.[13] Indeed, although a rodent astrocyte domain can reportedly cover up to 120,000 synapses, a human astrocyte domain can cover up to 2 million synapses, suggesting greater processing complexity in the latter species.[13] These and other species-specific features highlight the likelihood of human astrocytes to differ from rodent astrocytes in their contributions to brain function and brain dysfunction. Human astrocytes thus have important applications in studies of basic brain function, disease modeling and drug discovery.

[1]Stanley Center for Psychiatric Research, Broad Institute of MIT and Harvard, Cambridge, MA, USA

[2]Department of Stem Cell and Regenerative Biology, Harvard University, Cambridge, MA, USA

[3]Centre for Gene Therapy and Regenerative Medicine, King's College, London, UK

[4]Klarman Cell Observatory, Broad Institute of MIT and Harvard, Cambridge, MA, USA

[5]University of Helsinki, Helsinki, Finland

[6]Department of Genetics, Harvard Medical School, Boston, MA, USA

[7]These authors contributed equally

[8]Lead contact

*Correspondence: rnehme@broadinstitute.org (R.N.), lbarrett@broadinstitute.org (L.E.B.)

https://doi.org/10.1016/j.isci.2023.106995

With the emergence of human pluripotent stem cell (hPSC) technologies, it is now feasible to sustainably generate an array of brain cell types *in vitro*. Notably, numerous studies have shown that glial cells are necessary for the functional maturation of neurons.[15–17] For practical considerations and ease of access, most studies supplement neuronal cultures with rodent astrocytes, and more recently, commercially available primary fetal astrocytes. However, these approaches have significant limitations. As discussed above, rodent astrocytes diverge morphologically, transcriptionally and functionally from human astrocytes and do not allow for the investigation of the effect of human genetic variants and perturbations on biology and disease. Primary fetal astrocytes are not a sustainable resource and generally do not allow for the study of specific human genotypes of interest.

Recognizing the utility of human *in vitro* derived astrocytes, several protocols have been developed including those following a protracted developmental time-course in 3-dimensions (up to 20 months)[18] and more rapid 2-dimensional protocols.[19–23] Although these protocols produce cells expressing canonical astrocyte markers and are capable of recapitulating key functions such as responding to pro-inflammatory stimuli, much remains to be determined regarding: (i) the precise cell types and cell stages being generated and/or how closely they resemble fetal or adult human astrocytes from primary cultures or postmortem preparations, (ii) the robustness of protocols across individual hPSC lines, and (iii) their utility for disease modeling applications. Furthermore, most deeply characterized approaches are either lengthy or technically complicated, involving multiple experimental steps, such as purification, replating, and culturing in different formats, rendering such protocols less amenable to implementation across multiple cell lines and manipulations.
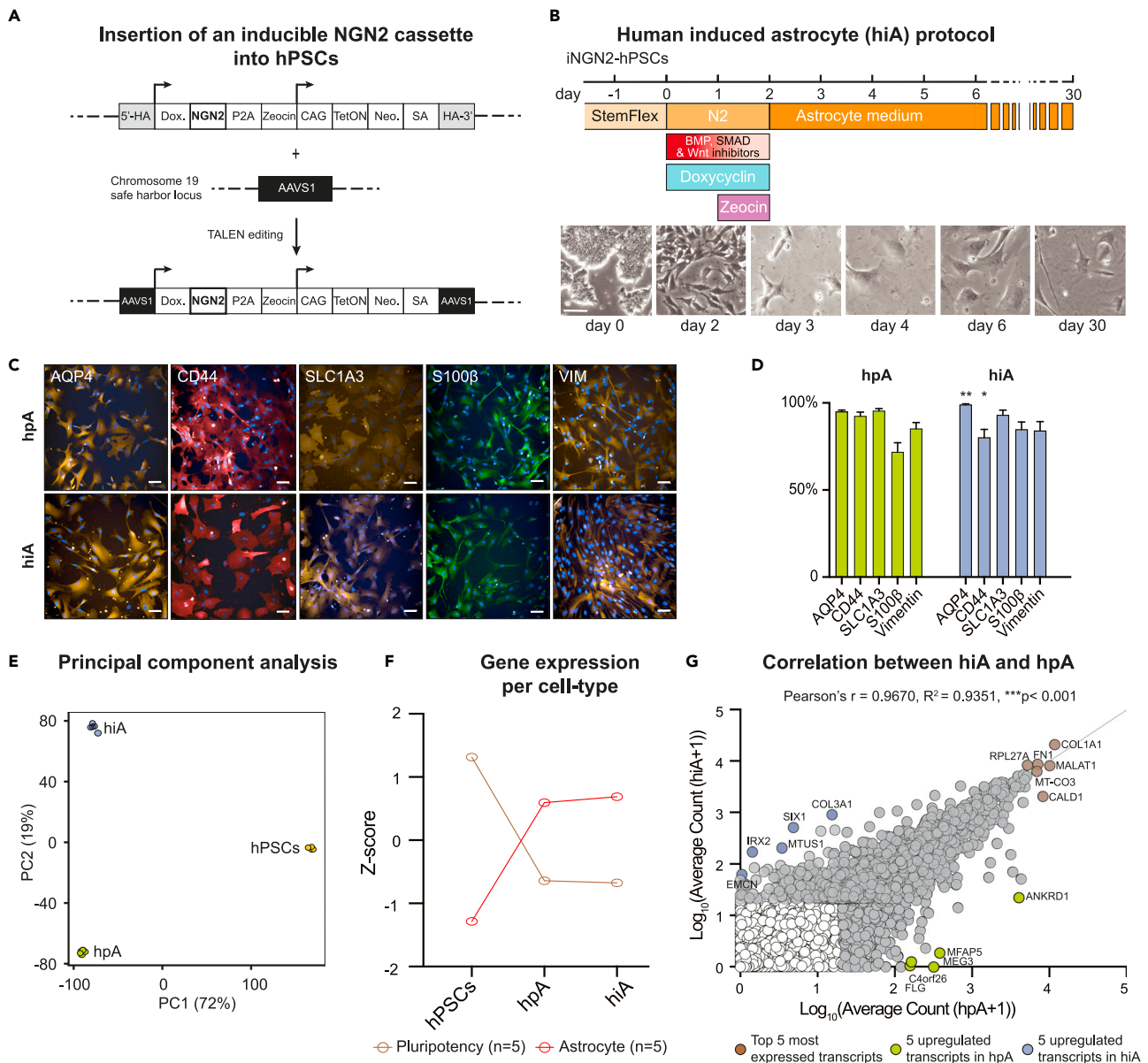
Several astrocyte differentiation protocols have recognized the importance of robust neural progenitor cell (NPC) generation as an important foundation for efficient astrocyte differentiation.[22,23] Here, we leveraged previous studies showing that NGN2 patterning with or without dual-SMAD and WNT inhibition can direct hPSCs toward diverse neural fates including forebrain neurons and peripheral neurons[15,24–26] and identifying optimal media conditions to differentiate NPCs into astrocytes.[22] Specifically, to generate NPCs we used transient NGN2 induction combined with dual-SMAD inhibition (SB431542, LDN-193189) and WNT inhibition (XAV939), previously shown to support forebrain patterning of the NPCs[15,25] followed by maturation in astrocyte media (ScienCell) previously screened for efficient differentiation of hPSC-derived forebrain NPCs into astrocytes.[22] This combination resulted in robust generation of astrocytes by 30 days *in vitro*. We then benchmarked our human induced astrocytes (hiAs) against human primary fetal astrocytes (hpAs) using a combination of immunophenotyping, RNA-sequencing and a series of functional assays assessing response to pro-inflammatory stimuli, ATP-induced calcium release and presynaptic development on neuronal co-culture. Although single-cell RNA-sequencing (scRNAseq) of *in vitro* derived astrocytes has been limited to 3-dimensional protocols,[18,27] requiring dual transcription factor over-expression approaches[28] or following FACS-purification,[29] we used scRNAseq analyses of our rapid 2-dimensional protocol from eight unique parental cell lines to define their molecular signatures. This revealed a striking degree of homogeneity at the single-cell level, and high reproducibility in the differentiated product across multiple parental cell lines. Finally, we generated hiAs in a model of trisomy 21 and recapitulated key features associated with the disease.

Collectively, these analyses establish a rapid, scalable, and reproducible differentiation protocol to generate homogeneous human astrocytes with a well-defined molecular signature, with limited interventions, which can be applied to many parental cell lines and specifically for the purposes of disease modeling.

RESULTS

Robust and rapid generation of human induced astrocytes (hiAs) from NPCs

To generate hiAs, a doxycycline inducible NGN2 expression construct was introduced into hPSCs through TALEN-mediated stable integration into the AAVS1 safe-harbor locus (Figure 1A).[30] Following neomycin selection for construct integration, iNGN2-hPSCs were neuralized and dorsalized by switching to N2 medium with doxycycline and small molecule patterning for 48hrs to induce an NPC-like fate (Figure 1B).[15,25] hPSCs neuralized through ectopic expression of NGN2 alongside small molecule patterning have been well-characterized, express canonical markers for NPCs such as NESTIN, PAX6, FOXG1, and SOX1 as well as dorsal rather than posterior or ventral markers, and can be captured in this state for subsequent analyses as highlighted previously.[25,31] After 24 h of Zeocin selection for NGN2 induction, and for an

A Insertion of an inducible NGN2 cassette into hPSCs

B Human induced astrocyte (hiA) protocol

C

D

E Principal component analysis

F Gene expression per cell-type

G Correlation between hiA and hpA

Pearson's r = 0.9670, R^2 = 0.9351, ***$p < 0.001$

Figure 1. Robust and rapid generation of human induced astrocytes (hiAs) from NPCs

(A) Integration of an inducible NGN2 cassette in the safe harbor locus of hPSCs by TALEN editing.

(B) Schematic of the 30-day hiA differentiation protocol with brightfield images over the induction time-course shown below. Scale bar = 100μm.

(C) Representative immunofluorescence images for AQP4, CD44, SLC1A3, S100b and VIM from human primary astrocytes (top) and human induced astrocytes (bottom). Scale bar = 25μm.

(D) Quantification of each marker from hiAs and hpAs shown as % of DAPI+ cells. Data are represented as mean ± SEM, *$p < 0.05$, **$p < 0.01$; unpaired non-parametric Kolmogorov-Smirnov test hiA compared to hpA; n > 3 biological replicates, n = 3 technical replicates.

(E) Principal component analysis (PCA) of bulk RNA-seq data comparing hPSCs, hpAs and hiAs. Note that a majority of variance is explained by the comparison between hPSCs and astrocytes.

(F) Gene expression per cell type for hPSCs, hpAs and hiAs using canonical pluripotent and astrocyte related genes.

(G) Scatterplot showing a high positive correlation between hpA and hiA expressed transcripts (TPM >20, in gray). Brown circles highlight the top 5 most expressed transcripts shared between hiAs and hpAs, while green circles highlight 5 transcripts upregulated in hpAs alone and blue circles highlight 5 transcripts upregulated in hiAs alone. Pearson's r = 0.9670, R2 = 0.9351, ***$p < 0.001$.

additional 28+ days, cells were passaged and maintained in a commercially available astrocyte medium (ScienCell) previously shown to induce astrocyte morphology, the expression of astrocyte canonical markers, and ensure replicative competency.[22] As shown by previous work using a similar approach for hPSC-based astrocyte generation, the commercially available medium supported astrocyte maturation better than all other tested in-house recipes.[22] Indeed, by day 4 after induction, the differentiating iNGN2-NPCs acquired an astrocyte-like morphology, with flat, wide cell bodies beginning to form star-like projections (Figure 1B). By day 30, a vast majority of the differentiated cells, referred to as hiAs, expressed canonical astrocyte markers including Aquaporin 4 (AQP4), CD44, Solute Carrier family 1 member 3 (SLC1A3), S100 calcium binding protein B (S100B) and Vimentin (VIM) by immunofluorescence, paralleling results obtained with human primary astrocytes (hpAs)(Figures 1C and 1D). For example, 99.05% of hiAs and 95.12% of hpAs expressed AQP4, and 93.11% of hiAs and 95.62% of hpAs expressed SLC1A3 (Figure 1D).

To further explore the commitment of hPSCs to an astrocyte identity, we compared the bulk transcriptomic profiles of hiAs with those of hPSCs and hpAs (Table S1). Principal component analysis of all three cell types revealed that the vast majority of transcriptomic variance could be explained by the comparison between hPSCs and astrocytes (PC1: 72%) rather than between different astrocyte populations (PC2: 19%) (Figure 1E). In addition, gene expression per cell type revealed a similar trend of decreased pluripotency genes and increased astrocyte-related genes in both hpAs and hiAs (Figure 1F). We also observed a high positive correlation between hpA and hiA expressed transcripts (Pearson's r = 0.9670; Figure 1G) suggesting a similar landscape in global transcriptome, in contrast with the correlations between hiAs and hPSCs, or hpAs and hPSCs (Figure S1). Finally, PANTHER analysis of the top enriched pathways shared by hpAs and hiAs, in contrast to hPSCs, revealed canonical astrocyte signaling pathways such as VEGF, PDGF, angiogenesis and integrin signaling (Figure S1). Of interest, the top enriched pathways unique to hiAs over hpAs or unique to hpAs over hiAs were largely not astrocyte specific (Figure S1). Collectively, these analyses indicate that our hiAs harbor key molecular hallmarks of hpAs.

hiAs recapitulate key functional features of hpAs

We next sought to establish both cell autonomous and non-cell-autonomous functionality of hiAs as compared with hpAs, including the ability to secrete cytokines in response to pro-inflammatory stimuli, calcium oscillation dynamics in response to ATP and the capacity to promote presynaptic development of human *in vitro* derived neurons (hNs). The astrocyte response to pro-inflammatory stimuli is crucial for normal function, with dysfunction of the inflammatory response strongly implicated in disease.[2,32–34] We therefore challenged our hiAs as well as hpAs with TNFα cytokine and subsequently quantified the secretion of the pleiotropic cytokine interleukin 6 (IL-6). Specifically, hpAs and hiAs were treated with either 100 ng/mL TNFα or 0.1% BSA control and the harvested supernatant was used to measure secreted IL-6 by ELISA. As expected, both hiAs and hpAs showed a robust and significant response to TNFα stimulation compared to BSA control, with hiAs secreting IL-6 at levels slightly above hpAs (Figure 2A).
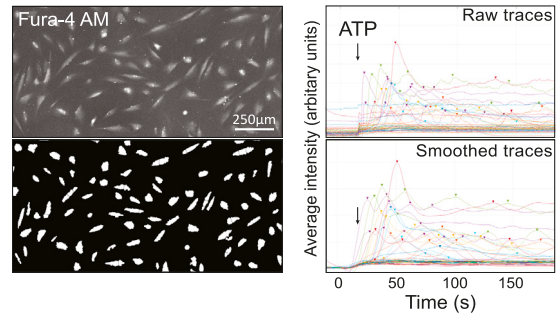
Astrocytes also display spikes of cytoplasmic calcium concentration as a response to mechanical, ATP or glutamate stimulation.[17,35,36] To assess the excitability of our hiAs and hpAs, we evaluated their response to ATP stimulation (Figures 2B–2E, Videos S1 and S2). Specifically, we used Fura-4 AM dye to image calcium concentration in the cytoplasm and recorded eight key features including: fluorescence level before and after stimulation as well as peak height, number, duration, rising time, falling time, peak interval and the area under the curve. Less than a minute following ATP administration both hiAs and hpAs sharply increased their cytoplasmic calcium concentration (Figure 2B) and displayed the same clusters of typical behavior with similar distributions overall (Figures 2C and S2). Data from both cell types were then pooled together and k-mean clustered (k = 5) (Figures 2C–2E). After separating cells based on their origin (hiA versus hpA), we also recovered similar signatures for each cluster (Figure 2E). Notably, individual traces of cells from any given cluster produced the same shape and did not depend on the sample of origin (Figure S2). These data support highly similar calcium dynamics between hiAs and hpAs.

Finally, astrocytes play critical roles in the establishment of synaptic networks, a key non-cell-autonomous function of astrocytes in the human brain. Previous studies have shown that both rodent and human astrocytes can improve the maturation of hNs.[15,19,20,30] Using an established glutamatergic hN differentiation protocol[15] combined with an automated synaptic quantification platform,[30] we analyzed presynaptic development in hN + hiA co-cultures derived from the same parental cell line, as well as hN + hpA
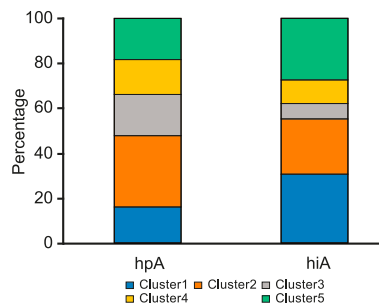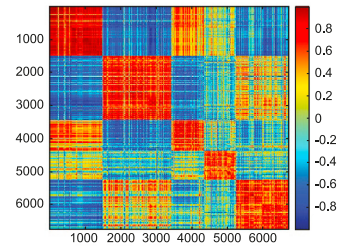
A Response to TNFα stimulation

BSA ☐
TNFα ☐
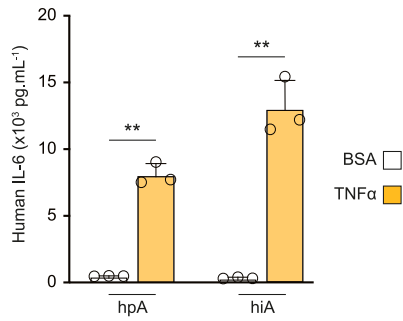
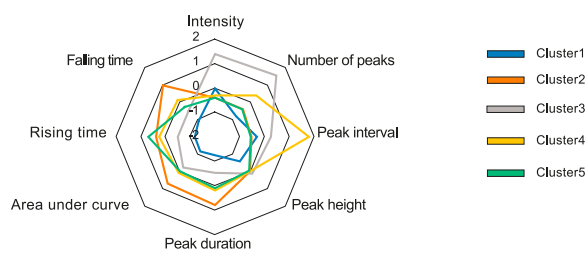**B** Representative image, mask and calcium concentration recordings

C Distribution of clusters across astrocytes

Cluster1 Cluster2 Cluster3
Cluster4 Cluster5
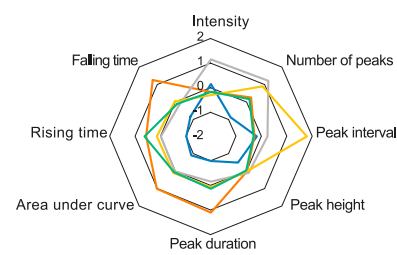
D Cell to cell correlation (pooled dataset)

E

hpA (Z-score)

Cluster1
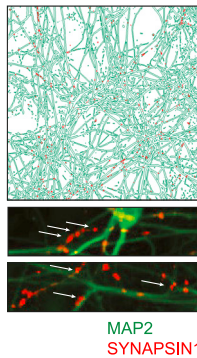Cluster2
Cluster3
Cluster4
Cluster5

hiA (Z-score)

F

hN + hpA co-culture
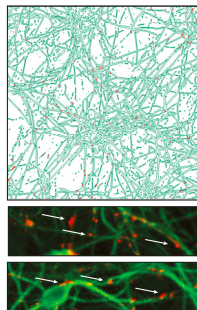
hN + hiA co-culture

MAP2
SYNAPSIN1
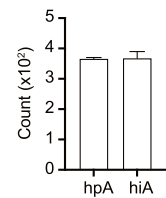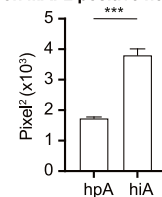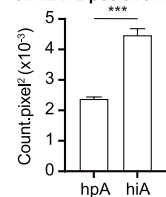
Area occupied by MAP2 positive neurites
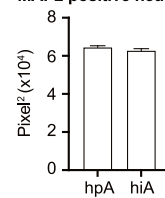
DAPI positive nuclei

Area occupied by SYNAPSIN1 puncta on MAP2 positive neurites

Density of SYNAPSIN1 puncta on MAP2 positive neurites

Figure 2. hiAs recapitulate key functional features of hpAs

(A) Bar graph showing human IL-6 detected from hiAs and hpAs by ELISA in response to 100 ng/mL human TNFa (orange) versus 0.1% BSA control (white) treatment. (Data are represented as mean ± SEM, **p < 0.01; One-way ANOVA with Tukey's multiple comparisons test; n = 3 biological replicates, n = 3 technical replicates).

(B) ATP-induced calcium release. Representative Fura-4 image of hiAs (top left), and associated mask (bottom left), raw traces (top right) and smoothed traces (bottom right). Intensity (arbitrary unit) is measured as an average on the surface of each cell. Arrow indicates timing of ATP stimulation. Scale bar = 250μm.

(C) Distribution of each cell population among the identified 5 clusters. Tables of Z-scored features were pulled together, clustered, then split into hpA and hiA.

(D) Correlation heatmap for 6,745 recorded cells. Correlation is computed on the table of Z-scored values for the eight identified features. Cells are sorted by cluster, then within each cluster, are sorted based on their sample of origin, showing that the correlation is strongly dependent on calcium signature but not sample.

(E) Radar plot of the mean Z-scored value taken by the 8 features used for clustering the data. Note that the shape of the typical signature of each cluster is the same for hpAs (left) and hiAs (right).

(F) Left, Representative CellProfiler output images of the two conditions (hN + hpA and hN + hiA) and representative pictures of SYNAPSIN1 puncta co-localized with MAP2 positive neurites (arrows point to presynaptic puncta). Right, Quantification of the area occupied by MAP2 positive neurites, the area occupied by SYNAPSIN1 puncta colocalized on MAP2 positive neurites, the number of DAPI positive nuclei and the density of SYNAPSIN1 puncta co-localized on MAP2 positive neurites in hN + hpA and hN + hiA co-cultures. Data are represented as mean ± SEM, n = 1 technical replicate, n = 60 biological replicates (wells) per condition, ***p < 0.001, unpaired t-test with Welch's correction.

co-cultures. Specifically, we quantified the presynaptic SYNAPSIN1 aggregates localized on and along the well described neuronal somato-dendritic marker MAP2 (microtubule-associated protein 2). These analyses revealed significant increases in the density and the area of presynaptic puncta opposed to MAP2-expressing neurites in hiA + hN as compared to hpA + hN co-culture, with no difference in the area occupied by MAP2 positive neurites or the number of DAPI positive nuclei detected. This is consistent with the ability of both hiAs and hpAs to support human presynaptic network development (Figure 2F).

Collectively, these results demonstrate that, compared to hpAs, our hiAs harbor similar immunocompetence, calcium transients in response to ATP and contributions to the development of neuronal networks.

Single-cell transcriptional profiling of hiAs from multiple donors

Some current hPSC based methods for astrocyte generation require purification steps such as FACS to isolate a specific population of interest given the heterogeneity of cellular differentiation, and variability in the capacity of the differentiation to work effectively across a range of unique cell lines. To better understand the degree of homogeneity and reproducibility in our model, we performed scRNAseq on 8 unique parental cell lines (Table S2). To reduce technical variation, hiAs from each of the 8 donors were differentiated together in a "cell village" as previously described.[25] In brief, hiAs from each of the 8 cell lines were induced and initially differentiated separately, then mixed in equal numbers 25 days after induction to form a "village" and sequenced 5 days later (at day 30 after induction). Given the proliferative nature of the cells during the early stages of differentiation, we mixed cells from each donor later in their differentiation process relative to initial village methods in an effort to mitigate variability in growth rates impacting donor representation following sequencing. Each individual cell was then assigned to its donor-of-origin using transcribed single nucleotide polymorphisms (SNPs). Uniform Manifold Approximation and Projection (UMAP) showed high homogeneity across individual cell lines, with no cell line clustering distinctly from others using leiden unsupervised clustering (Figure 3A). Our scRNAseq analyses further confirmed that hiAs expressed canonical immature astrocytes markers including *VIM, GJA1, APOE, CD44, SLC1A3*, and *ID3* (Figure 3B). Given the propensity of *in vitro* differentiation protocols to have high heterogeneity and limited cell-type specificity, we explored whether using our NGN2 induction approach would produce oligodendrocyte or neuronal populations among our cells. We found that hiAs displayed minimal expression of common genes for NPCs, neurons, and oligodendrocytes and continued to express limited amounts of stem cell related genes (Figure 3C). To explore the variability across cell lines, we next compared the expression of canonical immature and mature astrocyte markers across donors, as well as global gene expression. Across all 8 cell lines, we observed a high degree of correlation of global expression across donors (Pearson's r = 0.96–0.98), highlighting the reproducibility of our method across a range of cell lines (Figure 3D).

Comparison of hiAs with *in vitro* and *ex vivo* astrocyte datasets

An important aim of *in vitro* models is to develop cellular substrates which resemble those found in the living human brain. To understand the similarities and differences among current iPSC-based astrocyte protocols, we compared our hiAs with existing scRNAseq datasets (see STAR Methods;[27–29]). We found
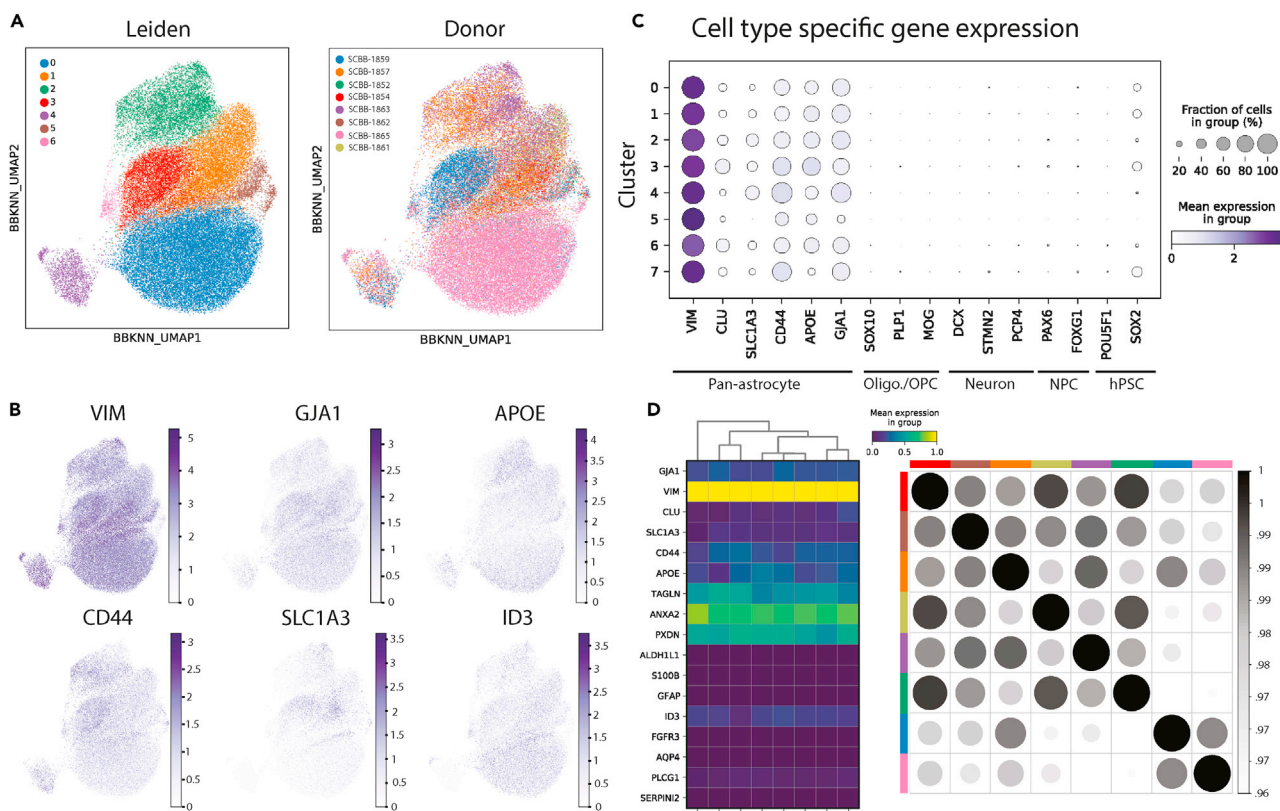
Figure 3. Single-cell transcriptional profiling of hiAs from multiple donors

(A) UMAP projection of scRNAseq data from 8 unique parental lines labeled by Left, cluster using Leiden unsupervised clustering and Right, cell line ID.

(B) Feature plot illustrating the distribution of canonical astrocyte markers VIM, GJA1, APOE, CD44, SLC1A3, and ID3 in UMAP space.

(C) Dot plot for markers of astrocytes (ID3, CLU, SLC1A3, CD44, APOE, GJA1), oligodendrocytes (SOX10, PLP1, MOG), excitatory neurons (DCX, STMN2, PCP4), neuronal progenitor cells (PAX6, FOXG1), and pluripotent stem cells (POU5F1, SOX2).

(D) Left, Matrix plot displaying average expression of canonical astrocyte markers by cell line. Right, correlation matrix of average expression across all genes between cell lines.

that UMAP displayed a high degree of similarity across each *in vitro* dataset with the majority of cells clustering together (Figures 4A and 4B). hiAs showed a high degree of homogeneity, with fewer sub-populations which clustered separately from the majority compared to other datasets (Figure 4C). We next compared the overall correlation of gene expression across iPSC-astrocyte models and found a moderate to high level of correlation (Pearson's r = 0.65–0.88) (Figure 4D). Although global expression across these datasets was similar, we wondered what genes were driving differences between them. We thus performed a differential expression analysis to compare across individual models. Genes contributing to differences across models were not specific for astrocyte identity or function, and included many mitochondrial and ribosomal genes (Figure 4E and Table S3). This illustrated that on average, each model resulted in comparable levels of expression of canonical astrocyte markers. Although this was true when exploring average expression, there were differences in canonical astrocyte gene expression patterns across clusters, where certain models populated greater proportions (Table S4). For example, cluster 9 showed elevated expression of immature astrocyte markers such as *TOP2A*, *CENPF* and *NUSAP1* relative to other clusters (Figure 4F). As shown in Figure 4C, cluster 9 predominantly contained cells from Leng et al. (2022),[28] although only representing ~0.2% of the total population. However, issues such as technical variation and limitations of sequencing depth may impact the detection and direct comparison of specific transcripts across datasets. We therefore examined expression across a large set of genes associated with astrocyte identity and behavior instead of focusing on single genes, creating a metagene score for each cell based on its contribution to expression of a set of genes associated with either astrocyte precursor cells or mature astrocytes as described by Zhang et al. (2016).[37] When we assessed the contribution of each model to these gene sets, we found that all models contributed similar amounts of RNA to both astrocyte precursor cell markers as
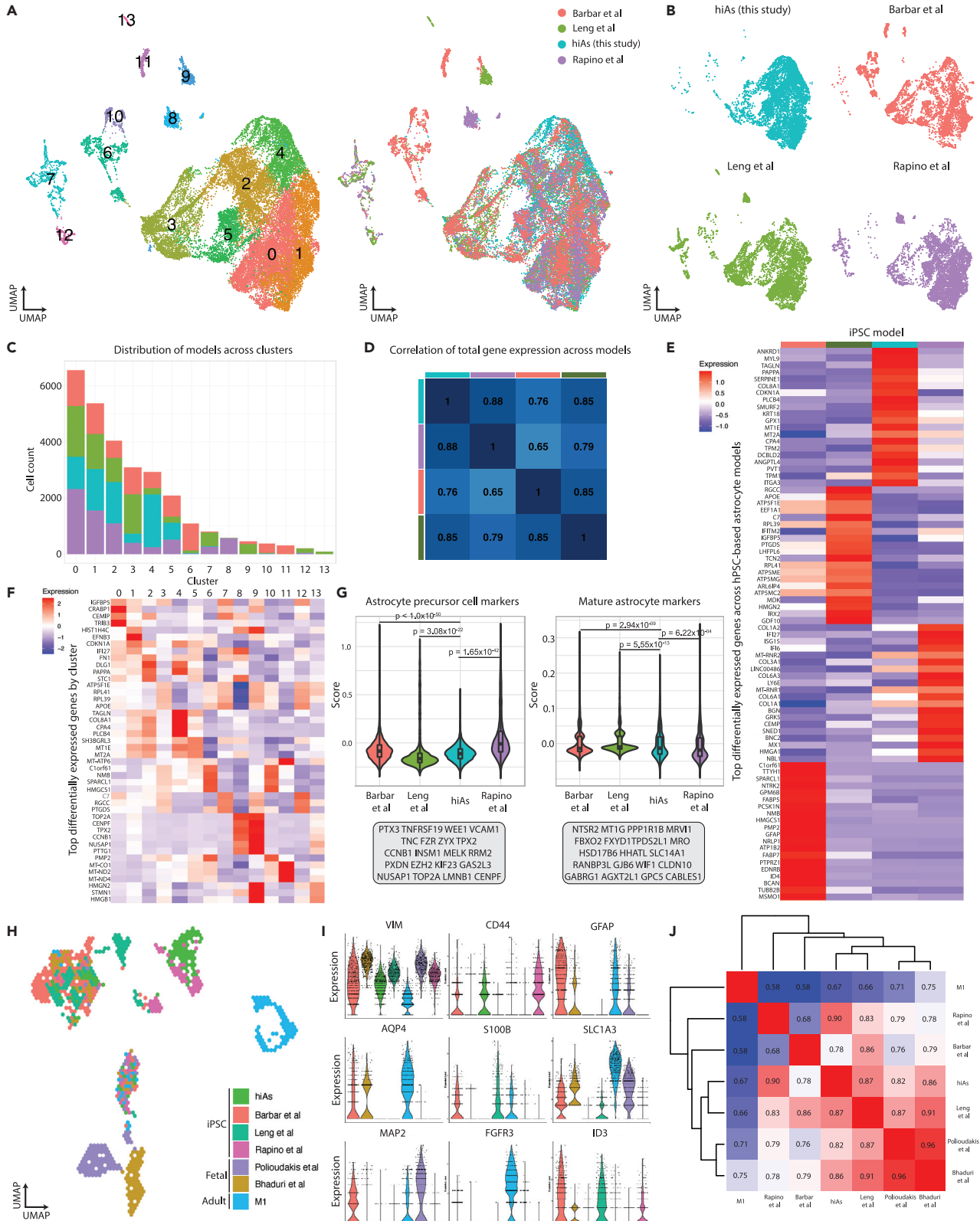
Figure 4. Comparison of hiAs with in vitro and ex vivo astrocyte datasets

(A) UMAP projection of scRNAseq data from four iPSC-astrocyte datasets (Barbar et al.,[29] Leng et al.,[28] Rapino et al.[27] and hiAs generated in this study) labeled by Left, cluster using Louvain unsupervised clustering and Right, by study.

(B) Left, top, UMAP projection only labeling hiA data. Left, bottom, UMAP projection only labeling Leng et al.[28] data. Right, top, UMAP projection labeling only Barbar et al.[29] data. Right, bottom, UMAP projection labeling only Rapino et al.[27] data.

(C) Distribution of cells from each iPSC-astrocyte dataset by cluster.

(D) Correlation of average gene expression across all iPSC-astrocyte models.

(E) Top 20 differentially expressed genes in each iPSC-astrocyte dataset.

(F) Top 4 differentially expressed genes in each cluster.

(G) Left, Metagene enrichment score for astrocyte precursor markers across iPSC-astrocyte datasets. p value = 0.006, ANOVA. right, Metagene enrichment score for mature astrocyte markers across iPSC-astrocyte datasets. p value <0.005, ANOVA. Data are represented as mean ± SEM.

(H) UMAP projection of iPSC-astrocyte datasets integrated with fetal and postmortem human brain data labeled by dataset.

(I) Expression of canonical astrocyte markers (VIM, CD44, GFAP, AQP4, S100B, SLC1A3, MAP2, FGFR3, and ID3) across iPSC-astrocyte and human brain datasets.

(J) Canonical correlation analysis of iPSC-astrocytes and human brain datasets for average global gene expression.

well as mature astrocyte markers (Figure 4G). Consistent with these findings, hiAs showed lower standard deviations than their counterparts, further illustrating the homogeneity of our cells in their contribution to the expression of these specific markers compared to the other iPSC astrocyte models.

To understand the *in vivo* fidelity of our system as well as other iPSC-based astrocyte models, we integrated our scRNAseq data and published datasets with existing data from the fetal human brain prefrontal cortex[38,39] and M1 motor cortex from postmortem adult brain.[40] UMAP analysis revealed similar clustering between *in vitro* datasets, with some clusters including cells from the two fetal datasets and the M1 atlas used in the analysis (Figure 4H). Although some cells generated from each method overlapped with a subset of cells from the human brain tissues, most cells from the fetal and postmortem datasets clustered separately (Figure 4H). We also observed the same pattern when including hpAs (derived from fetal tissue) in the analyses (Figure S3). Similar to hiAs and other iPSC-astrocytes, hpAs also failed to cluster with data from the fetal cortex or postmortem data (Figure S3A), consistent with the high correlation we had noted between the gene expression profiles of hiAs and hpAs (Figure 1). The expression of some canonical astrocyte genes varied across the brain and stem cell-based datasets (Figure 4I). For instance, *AQP4* and *FGFR3* were more strongly expressed in human adult astrocytes compared to human primary fetal or stem cell derived astrocytes, whereas *VIM* was robustly expressed across all datasets (Figure 4I). Of interest, we noticed discordance between the protein and mRNA abundance for several canonical astrocyte markers such as AQP4, SLC1A3, and S100B in our hiAs (Figures 1C and 4I). Indeed, despite low transcript levels for these genes, we could reliably detect the presence of the protein (Figure 1C). This phenotype was also observed in the human primary astrocytes (Figure S3B). We further compared the average expression across all genes between *in vitro* datasets and the human brain. When looking at the correlation of global gene expression across datasets, hiAs exhibit relatively high correlation with the fetal brain data, and a moderate correlation with the M1 atlas data (Pearson's r = 0.82, 0.86, 0.67, respectively) (Figure 4J). Importantly, although other iPSC-based astrocyte models exhibited similar correlations to these specific human brain datasets, hiAs showed the strongest correlation to the M1 atlas data relative to other *in vitro* models (Pearson's r = 0.67) (Figure 4J). Based on these analyses, we hypothesized that longer term culture of hiAs might further mature them. Transcriptomic analysis from hiAs cultured until D60 showed modest changes in gene expression space, and a small increase in correlation to the human brain datasets, suggesting hiAs exhibit a small increase in maturity with additional time in culture (Figures S4A–S4D). In addition, we leveraged a published dataset of the same NGN2-driven NPC-like cells at day two[25] to examine the molecular trajectory of iPSCs, NPCs and hiAs as compared with hpAs (Figure S4E). Here, we observed an increase in early astrocyte fate regulators including *NFIA*, *NFIB* and *SOX9* in hiAs and hpAs as compared with NPCs and iPSCs (Figure S4E). When assessing transcription factors implicated in astrocyte maturation,[41] we detect modest induction of *RORB* and *LHX2*, and no induction of *DBX2* and *FEZF2* in either hiAs or hpAs (Figure S4F). Overall, our data suggested that hiAs closely resembled other iPSC-derived astrocytes and exhibited reasonable correlation to relevant human brain datasets from the prefrontal and motor cortex, presenting a robust model for investigating astrocyte biology as early as 30 days after induction.

hiAs capture disease phenotypes in model of trisomy 21

We next sought to establish the utility of our hiA protocol for disease modeling, given the high relevance of this application. Specifically, numerous studies have shown deficits in astrocytes due to triplication of
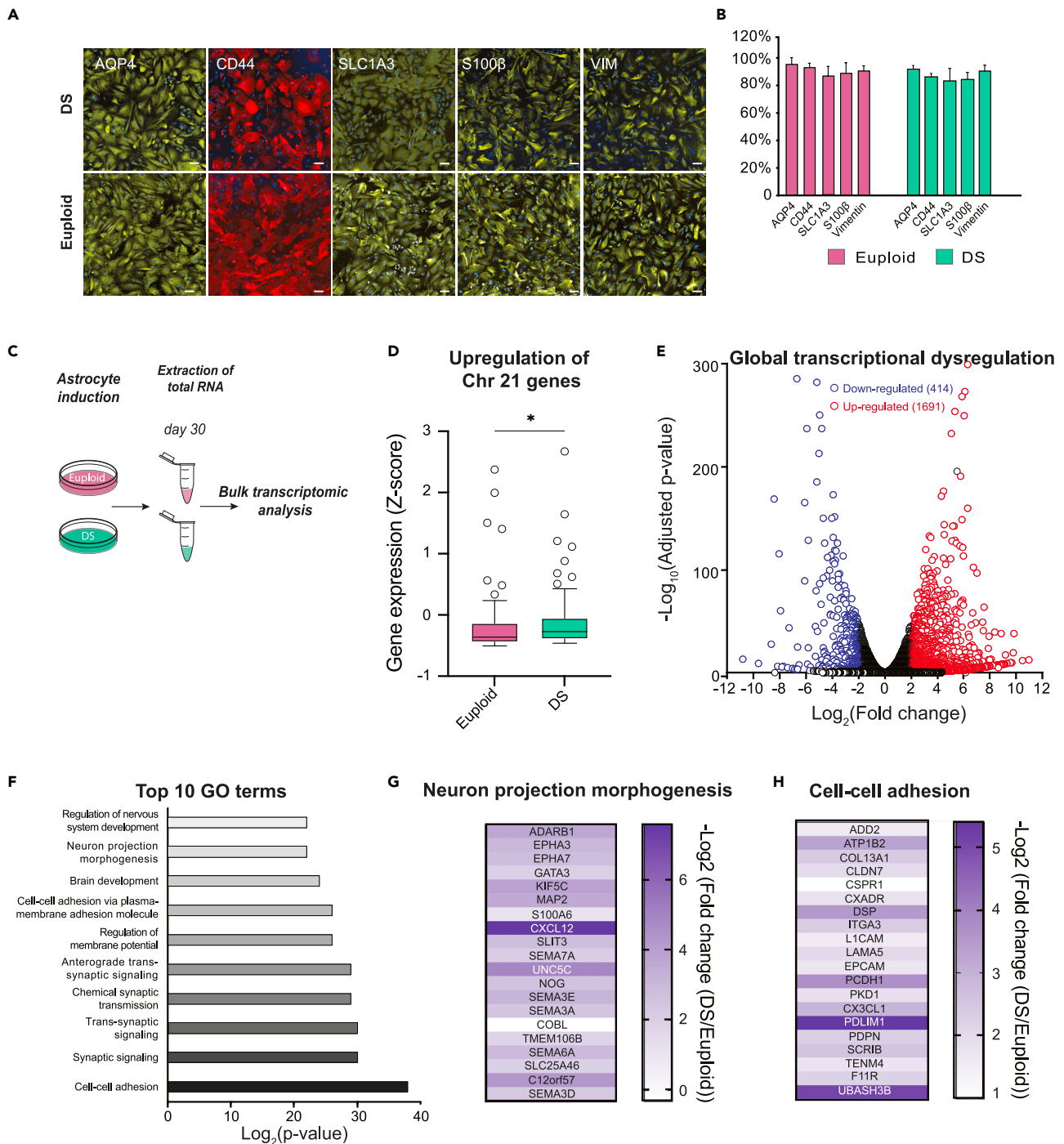
Figure 5. hiAs capture disease phenotypes in model of trisomy 21

(A) Representative immunofluorescence images for AQP4, CD44, SLC1A3, S100b and VIM from astrocytes derived from DS patient cells (DS1) and astrocytes derived from euploid control cells (DS2U). Scale bar = 100 μm.

(B) Quantification of each marker from DS and euploid astrocytes shown as percentage of DAPI positive cells. Data are represented as mean ± SEM. n > 3 biological replicates, n = 3 technical replicates.

(C) Schematic of bulk transcriptional analyses for DS and euploid astrocytes.

(D) Gene expression Z-scores for 77 genes encoded on chromosome 21 from DS versus euploid control cells. Data are represented mean ± SEM, *p = 0.0142, Mann Whitney two-tailed t test.

Figure 5. *Continued*

(E) Volcano plot showing wide dysregulation of the transcriptome in DS astrocytes compared to isogenic euploid controls, with a bias toward upregulation. Significantly down-regulated genes are shown in blue and significantly up-regulated genes are shown in red. Log2FC is shown on the x axis and the -log10 of the adjusted p value is shown on the y axis.

(F) The top ten biological processes identified as enriched in differentially expressed genes, as calculated by Gene Ontology (GO) analysis performed via Metascape. The Log2 of the p value is shown on the x axis.

(G and H), Heat maps showing examples of genes from the 'neuron projection morphogenesis' (left) and 'cell-cell adhesion' (right) GO terms identified in (F). Scale shows the -log2FC of DS versus euploid control.

chromosome 21, which drives Down syndrome.[42–46] For example, using iPSC-derived astrocytes, Chen et al. (2014)[43] found that trisomy 21 drove global transcriptional perturbations as well as higher levels of reactive oxygen species and reduced expression of pro-synaptic factors compared to euploid astrocytes. Also using iPSC-derived astrocytes, Bally et al. (2020)[45] identified global transcriptional perturbations due to trisomy 21 coupled with chromatin accessibility analyses, revealing alterations to axon development, extracellular matrix organization and cell adhesion.[45] We therefore generated hiAs from an isogenic pair of commercially available iPSC lines with and without trisomy 21,[47] referred to as DS1 (trisomy 21) and DS2U (euploid) hiAs (Table S5). As expected, hiAs derived from both euploid and trisomy 21 iPSCs expressed canonical astrocyte markers (Figures 5A and 5B), in accordance with our previous analyses of a control cell line (Figures 1C and 1D). Given the high degree of homogeneity observed in our scRNAseq datasets (Figures 3 and 4), we then extracted RNA for bulk transcriptional analyses (Figure 5C). As expected, a majority of expressed genes such as *COL18A1, COL6A, BACE2* and *ADARB1*, encoded on chromosome 21 (HSA21) were upregulated in trisomy 21 hiAs compared with euploid control hiAs, with a median fold change of 1.4931 as compared to 0.9623 obtained with the same analysis performed on chromosome 3 (Figures 5D and S5). Also, using a p_{adj} threshold of 0.05 and a log_2FC threshold of $+/-2$, we observed global transcriptional perturbations, detecting 1691 significantly upregulated genes and 414 significantly downregulated genes due to trisomy 21 (Figure 5E). GO term analyses of the differentially expressed genes revealed biological processes such as cell-cell adhesion, synaptic signaling and neuron projection morphogenesis (Figure 5F), consistent with previous studies of cell-autonomous astrocyte dysfunction as well as deleterious impacts on neuronal and synaptic development in Down syndrome; of note, our analyses captured astrocyte phenotypes also detected in a 160+ day astrocyte differentiation protocol.[45] Examples of individual genes involved in neuron projection morphogenesis and cell-cell adhesion are highlighted in Figures 5G and 5H. These data support the expected transcriptional dysregulation of hiAs when used in a model of trisomy 21.

DISCUSSION

Despite their essentiality for modeling normal brain function as well as dysfunction in disease, glial cell types have lagged somewhat behind neuronal cell types when it comes to hPSC-based differentiation technologies. Protracted astrocyte differentiation protocols as well as those requiring 3-dimensional culture or additional purification steps complicate their utility for multi-cell line, adequately powered functional studies. Here, we present a simplified, rapid and robust protocol to generate homogeneous astrocytes with detailed molecular and functional benchmarking compatible with many parental cell lines and for disease modeling applications. These astrocytes, generated through a simple protocol driven by transient NGN2 expression produce inflammatory responses, elicit calcium signaling, and have pro-maturational effects on iPSC derived neurons. Furthermore, they are transcriptionally concordant with human primary astrocytes, a common *in vitro* model used to study human astrocyte biology, show a great degree of overlap with existing *in vitro* astrocyte approaches which often require longer culture times or more elaborate interventions to isolate specific cell populations, and display strong correlations with existing human brain datasets. Finally, the hiA cell population is functionally and transcriptionally homogeneous rendering this approach amenable to genetic or pharmacological perturbation screens and circumventing the need for costly single cell sequencing approaches. These features will facilitate the study of human astrocytes for disease modeling and drug screening applications.

In the future, we see two key areas to build off from our current hiA differentiation protocol. First, given the high degree of reproducibility across parental cell lines as well as the ability to capture disease-relevant phenotypes and contribute to the maturation of neuronal networks, we see precision co-culture of hiAs with additional brain cell types as a logical next step. Indeed, the advantage of generating each relevant brain cell type separately is the ability to precisely control cell ratios, to generate highly reproducible preparations and to manipulate genotypes or employ genetically diverse parental cell lines to explore cell-type

specific effects on network function. We show here that our hiAs can be co-cultured with human neurons and similarly contribute to their development as hpAs, and future studies to incorporate additional brain cell types will facilitate study of a host of biological questions. Second, although hiAs possess key molecular and functional features of hpAs, similar to other iPSC-derived astrocytes, they more closely resemble fetal rather than adult human astrocytes. Thus, more needs to be done to enhance their maturation in order to study the role of human astrocytes in processes beyond early development. In this regard, it is interesting to note that additional time in culture only modestly improved hiA maturity, suggesting that additional extrinsic factors may be required for further maturation. Indeed, one possibility is that a more complex co-culture system including neurons or other glial cell types will be required to more accurately recapitulate the *in vivo* environment and further mature the hiAs. In this regard, we recently examined transcriptional changes induced by co-culturing human neurons with murine glia, revealing enhancement of synaptic gene expression programs in neurons and increased cell adhesion molecules in glia[3] consistent with the pro-maturational effects of glia on human neurons; it remains to be determined whether human neurons also have a pro-maturational effect on human astrocytes *in vitro*. It is also possible that additional gene networks may need to be activated in order to achieve a more mature astrocyte state, including the induction of key astrocyte fate regulators.

Limitations of the study

Although we have performed molecular and functional characterization of hiAs at day 30, additional studies will be required to understand the molecular trajectory from iPSCs to hiAs and the underlying mechanisms which drive fate conversion. Indeed, studies have identified epigenetic and transcriptional changes during astrocyte maturation using murine models[41] and it will be interesting to probe the extent to which similar mechanisms underlie human astrocyte maturation. Relatedly, our differentiation protocol relies on commercial astrocyte media, and the precise components driving astrocyte differentiation remain to be determined. In addition, our analyses were performed *in vitro*, and assessment of *in vivo* engraftment capacity as well as regional astrocyte identity would be of significant future interest.

STAR★METHODS

Detailed methods are provided in the online version of this paper and include the following:

- KEY RESOURCES TABLE
- RESOURCE AVAILABILITY
  ○ Lead contact
  ○ Materials availability
  ○ Data and code availability
- EXPERIMENTAL MODEL AND SUBJECT DETAILS
  ○ Cell culture
  ○ Human induced astrocyte (hiA) generation
  ○ Human primary astrocytes (hpAs)
- METHOD DETAILS
  ○ Immunocytochemistry
  ○ TNFα stimulation
  ○ hN generation and synapse quantification
  ○ Calcium imaging and analysis
  ○ 3′ DGE bulk mRNA-sequencing and analysis of hPSCs, hiAs and hpAs
  ○ Bulk mRNA-sequencing and analysis of DS1 and DS2U hiAs
  ○ scRNA-sequencing and donor assignment
  ○ scRNAseq analysis of villages and integrated datasets
- QUANTIFICATION AND STATISTICAL ANALYSIS

SUPPLEMENTAL INFORMATION

Supplemental information can be found online at https://doi.org/10.1016/j.isci.2023.106995.

AUTHOR CONTRIBUTIONS

M.H.B., M.T., R.N., and L.E.B. conceived the project and wrote and edited the manuscript, M.T. performed astrocyte differentiations for the brightfield imaging time-course and scRNAseq experiments and performed analyses with support from D.M. and S.A.M., M.H.B. generated and optimized the hiA protocol, performed immunocytochemistry, bulk RNA-seq, ELISA, and synaptic connectivity experiments and analyzed relevant data, V.V. and L.B. performed the astrocyte calcium release experiments, and L.B. performed the analysis with supervision from S.L.F., O.P., and A.N. assisted with bulk RNA-seq analysis, J.A.K., E.C., and D.T. assisted with astrocyte production and immunocytochemistry. Astrocyte data from Rapino et al. was obtained courtesy of F.R. and L.L.R. All authors discussed the results and edited the manuscript. S.A.M., R.N., and L.E.B. secured funding and oversaw experiments.

DECLARATION OF INTERESTS

L.L.R. is a founder of Elevian, Rejuveron, and Vesalius Therapeutics, a member of their scientific advisory boards and a private equity shareholder. All are interested in formulating approaches intended to treat diseases of the nervous system and other tissues. He is also on the advisory board of Alkahest, a Grifols company, focused on the plasma proteome and brain aging. None of these companies provided any financial support for the work in this paper. The remaining authors declare no competing interests.

REFERENCES

1. Allen, N.J., and Eroglu, C. (2017). Cell biology of astrocyte-synapse interactions. Neuron *96*, 697–708. https://doi.org/10.1016/j.neuron.2017.09.056.

2. Sofroniew, M.V., and Vinters, H.V. (2010). Astrocytes: biology and pathology. Acta Neuropathol. *119*, 7–35. https://doi.org/10.1007/s00401-009-0619-8.

3. Pietiläinen, O., Trehan, A., Meyer, D., Mitchell, J., Tegtmeyer, M., Valakh, V., Gebre, H., Chen, T., Vartiainen, E., Farhi, S.L., et al. (2023). Astrocytic cell adhesion genes linked to schizophrenia correlate with synaptic programs in neurons. Cell Rep. *42*, 111988. https://doi.org/10.1016/j.celrep.2022.111988.

4. Abbott, N.J., Rönnbäck, L., and Hansson, E. (2006). Astrocyte-endothelial interactions at the blood-brain barrier. Nat. Rev. Neurosci. *7*, 41–53. https://doi.org/10.1038/nrn1824.

5. Cucullo, L., McAllister, M.S., Kight, K., Krizanac-Bengez, L., Marroni, M., Mayberg, M.R., Stanness, K.A., and Janigro, D. (2002). A new dynamic in vitro model for the multidimensional study of astrocyte-endothelial cell interactions at the blood-brain barrier. Brain Res. *951*, 243–254. https://doi.org/10.1016/s0006-8993(02)03167-0.

6. Goldstein, G.W. (1988). Endothelial cell-astrocyte interactions. A cellular model of the blood-brain barrier. Ann. N. Y. Acad. Sci. *529*, 31–39. https://doi.org/10.1111/j.1749-6632.1988.tb51417.x.

7. Liu, L.R., Liu, J.C., Bao, J.S., Bai, Q.Q., and Wang, G.Q. (2020). Interaction of microglia and astrocytes in the neurovascular unit. Front. Immunol. *11*, 1024. https://doi.org/10.3389/fimmu.2020.01024.

8. Amaral, A.I., Meisingset, T.W., Kotter, M.R., and Sonnewald, U. (2013). Metabolic aspects of neuron-oligodendrocyte-astrocyte interactions. Front. Endocrinol. *4*, 54. https://doi.org/10.3389/fendo.2013.00054.

9. John, G.R. (2012). Investigation of astrocyte - oligodendrocyte interactions in human cultures. Methods Mol. Biol. *814*, 401–414. https://doi.org/10.1007/978-1-61779-452-0_27.

10. Magnotti, L.M., Goodenough, D.A., and Paul, D.L. (2011). Functional heterotypic interactions between astrocyte and oligodendrocyte connexins. Glia *59*, 26–34. https://doi.org/10.1002/glia.21073.

11. Hawrylycz, M.J., Lein, E.S., Guillozet-Bongaarts, A.L., Shen, E.H., Ng, L., Miller, J.A., van de Lagemaat, L.N., Smith, K.A., Ebbert, A., Riley, Z.L., et al. (2012). An anatomically comprehensive atlas of the adult human brain transcriptome. Nature *489*, 391–399. https://doi.org/10.1038/nature11405.

12. Han, X., Chen, M., Wang, F., Windrem, M., Wang, S., Shanz, S., Xu, Q., Oberheim, N.A., Bekar, L., Betstadt, S., et al. (2013). Forebrain engraftment by human glial progenitor cells enhances synaptic plasticity and learning in adult mice. Cell Stem Cell *12*, 342–353. https://doi.org/10.1016/j.stem.2012.12.015.

13. Oberheim, N.A., Wang, X., Goldman, S., and Nedergaard, M. (2006). Astrocytic complexity distinguishes the human brain. Trends Neurosci. *29*, 547–553. https://doi.org/10.1016/j.tins.2006.08.004.

14. Diniz, L.P., Almeida, J.C., Tortelli, V., Vargas Lopes, C., Setti-Perdigão, P., Stipursky, J., Kahn, S.A., Romão, L.F., de Miranda, J., Alves-Leon, S.V., et al. (2012). Astrocyte-induced synaptogenesis is mediated by transforming growth factor beta signaling through modulation of D-serine levels in cerebral cortex neurons. J. Biol. Chem. *287*, 41432–41445. https://doi.org/10.1074/jbc.M112.380824.

15. Nehme, R., Zuccaro, E., Ghosh, S.D., Li, C., Sherwood, J.L., Pietilainen, O., Barrett, L.E., Limone, F., Worringer, K.A., Kommineni, S., et al. (2018). Combining NGN2 programming with developmental patterning generates human excitatory neurons with NMDAR-mediated synaptic transmission. Cell Rep. *23*, 2509–2523.

16. Pfrieger, F.W., and Barres, B.A. (1997). Synaptic efficacy enhanced by glial cells

in vitro. Science *277*, 1684–1687. https://doi.org/10.1126/science.277.5332.1684.

17. Turovsky, E.A., Braga, A., Yu, Y., Esteras, N., Korsak, A., Theparambil, S.M., Hadjihambi, A., Hosford, P.S., Teschemacher, A.G., Marina, N., et al. (2020). Mechanosensory signaling in astrocytes. J. Neurosci. *40*, 9364–9371. https://doi.org/10.1523/JNEUROSCI.1249-20.2020.

18. Sloan, S.A., Darmanis, S., Huber, N., Khan, T.A., Birey, F., Caneda, C., Reimer, R., Quake, S.R., Barres, B.A., and Paşca, S.P. (2017). Human astrocyte maturation captured in 3D cerebral cortical spheroids derived from pluripotent stem cells. Neuron *95*, 779–790.e6. https://doi.org/10.1016/j.neuron.2017.07.035.

19. Canals, I., Ginisty, A., Quist, E., Timmerman, R., Fritze, J., Miskinyte, G., Monni, E., Hansen, M.G., Hidalgo, I., Bryder, D., et al. (2018). Rapid and efficient induction of functional astrocytes from human pluripotent stem cells. Nat. Methods *15*, 693–696. https://doi.org/10.1038/s41592-018-0103-2.

20. Hedegaard, A., Monzón-Sandoval, J., Newey, S.E., Whiteley, E.S., Webber, C., and Akerman, C.J. (2020). Pro-maturational effects of human iPSC-derived cortical astrocytes upon iPSC-derived cortical neurons. Stem Cell Rep. *15*, 38–51. https://doi.org/10.1016/j.stemcr.2020.05.003.

21. Santos, R., Vadodaria, K.C., Jaeger, B.N., Mei, A., Lefcochilos-Fogelquist, S., Mendes, A.P.D., Erikson, G., Shokhirev, M., Randolph-Moore, L., Fredlender, C., et al. (2017). Differentiation of inflammation-responsive astrocytes from glial progenitors generated from human induced pluripotent stem cells. Stem Cell Rep. *8*, 1757–1769. https://doi.org/10.1016/j.stemcr.2017.05.011.

22. Tcw, J., Wang, M., Pimenova, A.A., Bowles, K.R., Hartley, B.J., Lacin, E., Machlovi, S.I., Abdelaal, R., Karch, C.M., Phatnani, H., et al. (2017). An efficient platform for astrocyte differentiation from human induced pluripotent stem cells. Stem Cell Rep. *9*, 600–614. https://doi.org/10.1016/j.stemcr.2017.06.018.

23. Voulgaris, D., Nikolakopoulou, P., and Herland, A. (2022). Generation of Human iPSC-Derived Astrocytes with a mature star-shaped phenotype for CNS modeling. Stem Cell Rev. Rep. *18*, 2494–2512. https://doi.org/10.1007/s12015-022-10376-2.

24. Limone, F., Guerra San Juan, I., Mitchell, J.M., Smith, J.L.M., Raghunathan, K., Meyer, D., Ghosh, S.D., Couto, A., Klim, J.R., Joseph, B.J., et al. (2023). Efficient generation of lower induced motor neurons by coupling Ngn2 expression with developmental cues. Cell Rep. *42*, 111896. https://doi.org/10.1016/j.celrep.2022.111896.

25. Wells, M.F., Nemesh, J., Ghosh, S., Mitchell, J.M., Salick, M.R., Mello, C.J., Meyer, D., Pietilainen, O., Piccioni, F., Guss, E.J., et al. (2023). Natural variation in gene expression and viral susceptibility revealed by neural progenitor cell villages. Cell Stem Cell *30*, 312–332.e13. https://doi.org/10.1016/j.stem.2023.01.010.

26. Lin, H.C., He, Z., Ebert, S., Schörnig, M., Santel, M., Nikolova, M.T., Weigert, A., Hevers, W., Kasri, N.N., Taverna, E., et al. (2021). NGN2 induces diverse neuron types from human pluripotency. Stem Cell Rep. *16*, 2118–2127. https://doi.org/10.1016/j.stemcr.2021.07.006.

27. Rapino, F., Natoli, T., Limone, F., O'Connor, E., Blank, J., Tegtmeyer, M., Chen, W., Norabuena, E., Narula, J., Hazelbaker, D., et al. (2023). Small-molecule screen reveals pathways that regulate C4 secretion in stem cell-derived astrocytes. Stem Cell Rep. *18*, 237–253. https://doi.org/10.1016/j.stemcr.2022.11.018.

28. Leng, K., Rose, I.V.L., Kim, H., Xia, W., Romero-Fernandez, W., Rooney, B., Koontz, M., Li, E., Ao, Y., Wang, S., et al. (2022). CRISPRi screens in human iPSC-derived astrocytes elucidate regulators of distinct inflammatory reactive states. Nat. Neurosci. *25*, 1528–1542. https://doi.org/10.1038/s41593-022-01180-9.

29. Barbar, L., Rusielewicz, T., Zimmer, M., Kalpana, K., and Fossati, V. (2020). Isolation of human CD49f(+) astrocytes and in vitro iPSC-based neurotoxicity assays. STAR Protoc. *1*, 100172. https://doi.org/10.1016/j.xpro.2020.100172.

30. Berryer, M.H., Rizki, G., Nathanson, A., Klein, J.A., Trendafilova, D., Susco, S.G., Lam, D., Messana, A., Holton, K.M., Karhohs, K.W., et al. (2023). High-content synaptic phenotyping in human cellular models reveals a role for BET proteins in synapse assembly. Elife *12*, e80168. https://doi.org/10.7554/eLife.80168.

31. Nehme, R., Pietiläinen, O., Artomov, M., Tegtmeyer, M., Valakh, V., Lehtonen, L., Bell, C., Singh, T., Trehan, A., Sherwood, J., et al. (2022). The 22q11.2 region regulates presynaptic gene-products linked to schizophrenia. Nat. Commun. *13*, 3690. https://doi.org/10.1038/s41467-022-31436-8.

32. Kam, T.I., Hinkle, J.T., Dawson, T.M., and Dawson, V.L. (2020). Microglia and astrocyte dysfunction in Parkinson's disease. Neurobiol. Dis. *144*, 105028. https://doi.org/10.1016/j.nbd.2020.105028.

33. Leal, M.C., Casabona, J.C., Puntel, M., and Pitossi, F.J. (2013). Interleukin-1beta and tumor necrosis factor-alpha: reliable targets for protective therapies in Parkinson's Disease? Front. Cell. Neurosci. *7*, 53. https://doi.org/10.3389/fncel.2013.00053.

34. Liddelow, S.A., and Barres, B.A. (2017). Reactive astrocytes: production, function, and therapeutic potential. Immunity *46*, 957–967. https://doi.org/10.1016/j.immuni.2017.06.006.

35. Allen, M., Huang, B.S., Notaras, M.J., Lodhi, A., Barrio-Alonso, E., Lituma, P.J., Wolujewicz, P., Witztum, J., Longo, F., Chen, M., et al. (2022). Astrocytes derived from ASD individuals alter behavior and destabilize neuronal activity through aberrant Ca(2+) signaling. Mol. Psychiatry *27*, 2470–2484. https://doi.org/10.1038/s41380-022-01486-x.

36. Fujii, Y., Maekawa, S., and Morita, M. (2017). Astrocyte calcium waves propagate proximally by gap junction and distally by extracellular diffusion of ATP released from volume-regulated anion channels. Sci. Rep. *7*, 13115. https://doi.org/10.1038/s41598-017-13243-0.

37. Zhang, Y., Sloan, S.A., Clarke, L.E., Caneda, C., Plaza, C.A., Blumenthal, P.D., Vogel, H., Steinberg, G.K., Edwards, M.S.B., Li, G., et al. (2016). Purification and characterization of progenitor and mature human astrocytes reveals transcriptional and functional differences with mouse. Neuron *89*, 37–53. https://doi.org/10.1016/j.neuron.2015.11.013.

38. Bhaduri, A., Sandoval-Espinosa, C., Otero-Garcia, M., Oh, I., Yin, R., Eze, U.C., Nowakowski, T.J., and Kriegstein, A.R. (2021). An atlas of cortical arealization identifies dynamic molecular signatures. Nature *598*, 200–204. https://doi.org/10.1038/s41586-021-03910-8.

39. Polioudakis, D., de la Torre-Ubieta, L., Langerman, J., Elkins, A.G., Shi, X., Stein, J.L., Vuong, C.K., Nichterwitz, S., Gevorgian, M., Opland, C.K., et al. (2019). A single-cell transcriptomic atlas of human neocortical development during mid-gestation. Neuron *103*, 785–801.e8. https://doi.org/10.1016/j.neuron.2019.06.011.

40. BRAIN Initiative Cell Census Network BICCN (2021). A multimodal cell census and atlas of the mammalian primary motor cortex. Nature *598*, 86–102. https://doi.org/10.1038/s41586-021-03950-0.

41. Lattke, M., Goldstone, R., Ellis, J.K., Boeing, S., Jurado-Arjona, J., Marichal, N., MacRae, J.I., Berninger, B., and Guillemot, F. (2021). Extensive transcriptional and chromatin changes underlie astrocyte maturation in vivo and in culture. Nat. Commun. *12*, 4335. https://doi.org/10.1038/s41467-021-24624-5.

42. Araujo, B.H.S., Kaid, C., De Souza, J.S., Gomes da Silva, S., Goulart, E., Caires, L.C.J., Musso, C.M., Torres, L.B., Ferrasa, A., Herai, R., et al. (2018). Down syndrome iPSC-derived astrocytes impair neuronal synaptogenesis and the mTOR pathway in vitro. Mol. Neurobiol. *55*, 5962–5975. https://doi.org/10.1007/s12035-017-0818-6.

43. Chen, C., Jiang, P., Xue, H., Peterson, S.E., Tran, H.T., McCann, A.E., Parast, M.M., Li, S., Pleasure, D.E., Laurent, L.C., et al. (2014). Role of astroglia in Down's syndrome revealed by patient-derived human-induced pluripotent stem cells. Nat. Commun. *5*, 4430. https://doi.org/10.1038/ncomms5430.

44. Mizuno, G.O., Wang, Y., Shi, G., Wang, Y., Sun, J., Papadopoulos, S., Broussard, G.J., Unger, E.K., Deng, W., Weick, J., et al. (2018). Aberrant calcium signaling in astrocytes inhibits neuronal excitability in a human down syndrome stem cell model. Cell Rep. *24*, 355–365. https://doi.org/10.1016/j.celrep.2018.06.033.

45. Ponroy Bally, B., Farmer, W.T., Jones, E.V., Jessa, S., Kacerovsky, J.B., Mayran, A., Peng, H., Lefebvre, J.L., Drouin, J., Hayer, A., et al. (2020). Human iPSC-derived Down syndrome

astrocytes display genome-wide perturbations in gene expression, an altered adhesion profile, and increased cellular dynamics. Hum. Mol. Genet. 29, 785–802. https://doi.org/10.1093/hmg/ddaa003.

46. Ponroy Bally, B., and Murai, K.K. (2021). Astrocytes in down syndrome across the lifespan. Front. Cell. Neurosci. 15, 702685. https://doi.org/10.3389/fncel.2021.702685.

47. Weick, J.P., Held, D.L., Bonadurer, G.F., 3rd, Doers, M.E., Liu, Y., Maguire, C., Clark, A., Knackert, J.A., Molinarolo, K., Musser, M., et al. (2013). Deficits in human trisomy 21 iPSCs and neurons. Proc. Natl. Acad. Sci. USA 110, 9962–9967. https://doi.org/10.1073/pnas.1216575110.

48. Thomson, J.A., Itskovitz-Eldor, J., Shapiro, S.S., Waknitz, M.A., Swiergiel, J.J., Marshall, V.S., and Jones, J.M. (1998). Embryonic stem cell lines derived from human blastocysts. Science 282, 1145–1147.

49. Zhang, Y., Pak, C., Han, Y., Ahlenius, H., Zhang, Z., Chanda, S., Marro, S., Patzke, C., Acuna, C., Covy, J., et al. (2013). Rapid single-step induction of functional neurons from human pluripotent stem cells. Neuron 78, 785–798. https://doi.org/10.1016/j.neuron.2013.05.029.

50. Xiong, Y., Soumillon, M., Wu, J., Hansen, J., Hu, B., van Hasselt, J.G.C., Jayaraman, G., Lim, R., Bouhaddou, M., Ornelas, L., et al. (2017). A comparison of mRNA sequencing with random primed and 3′-directed libraries. Sci. Rep. 7, 14626. https://doi.org/10.1038/s41598-017-14892-x.

51. Anders, S., Pyl, P.T., and Huber, W. (2015). HTSeq–a Python framework to work with high-throughput sequencing data. Bioinformatics 31, 166–169. https://doi.org/10.1093/bioinformatics/btu638.

52. Dobin, A., Davis, C.A., Schlesinger, F., Drenkow, J., Zaleski, C., Jha, S., Batut, P., Chaisson, M., and Gingeras, T.R. (2013). STAR: ultrafast universal RNA-seq aligner. Bioinformatics 29, 15–21. https://doi.org/10.1093/bioinformatics/bts635.

53. Robinson, M.D., McCarthy, D.J., and Smyth, G.K. (2010). edgeR: a Bioconductor package for differential expression analysis of digital gene expression data. Bioinformatics 26, 139–140. https://doi.org/10.1093/bioinformatics/btp616.

54. Love, M.I., Huber, W., and Anders, S. (2014). Moderated estimation of fold change and dispersion for RNA-seq data with DESeq2. Genome Biol. 15, 550. https://doi.org/10.1186/s13059-014-0550-8.

55. Cornwell, M., Vangala, M., Taing, L., Herbert, Z., Köster, J., Li, B., Sun, H., Li, T., Zhang, J., Qiu, X., et al. (2018). VIPER: visualization Pipeline for RNA-seq, a Snakemake workflow for efficient and complete RNA-seq analysis. BMC Bioinformatics 19, 135. https://doi.org/10.1186/s12859-018-2139-9.

56. Zhou, Y., Zhou, B., Pache, L., Chang, M., Khodabakhshi, A.H., Tanaseichuk, O., Benner, C., and Chanda, S.K. (2019). Metascape provides a biologist-oriented resource for the analysis of systems-level datasets. Nat. Commun. 10, 1523. https://doi.org/10.1038/s41467-019-09234-6.

57. Macosko, E.Z., Basu, A., Satija, R., Nemesh, J., Shekhar, K., Goldman, M., Tirosh, I., Bialas, A.R., Kamitaki, N., Martersteck, E.M., et al. (2015). Highly parallel genome-wide expression profiling of individual cells using nanoliter droplets. Cell 161, 1202–1214. https://doi.org/10.1016/j.cell.2015.05.002.

58. Polański, K., Young, M.D., Miao, Z., Meyer, K.B., Teichmann, S.A., and Park, J.E. (2020). BBKNN: fast batch alignment of single cell transcriptomes. Bioinformatics 36, 964–965. https://doi.org/10.1093/bioinformatics/btz625.

59. Hafemeister, C., and Satija, R. (2019). Normalization and variance stabilization of single-cell RNA-seq data using regularized negative binomial regression. Genome Biol. 20, 296. https://doi.org/10.1186/s13059-019-1874-1.

60. Welch, J.D., Kozareva, V., Ferreira, A., Vanderburg, C., Martin, C., and Macosko, E.Z. (2019). Single-cell multi-omic integration compares and contrasts features of brain cell identity. Cell 177, 1873–1887.e17. https://doi.org/10.1016/j.cell.2019.05.006.

STAR★METHODS

KEY RESOURCES TABLE

REAGENT or RESOURCE	SOURCE	IDENTIFIER
Antibodies		
Rabbit polyclonal anti-Aquaporin 4	Millipore	Cat# AB3594 RRID:AB_91530
Rat monoclonal anti-CD44	Thermo Fisher Scientific	Cat# 14-0441-82 RRID:AB_467246
Rabbit polyclonal anti-SLC1A3	Boster Biological Technology	Cat# PA2185 RRID:AB_2665510
Rabbit monoclonal anti-S100b	Abcam	Cat# ab52642 RRID:AB_882426
Rabbit polyclonal anti-Vimentin	Cell Signaling Technology	Cat# 3932S RRID:AB_2288553
Rabbit polyclonal anti-Synapsin1	Millipore	Cat# AB1543 RRID:AB_2200400
Chicken polyclonal anti-MAP2	Abcam	Cat# 5392 RRID:AB_2138153
Chemicals, peptides, and recombinant proteins		
TNF alpha	Sigma-Aldrich	Cat# H8916
Geltrex	Thermo Fisher Scientific	Cat# A1413302
Normocin	Invivogen	Cat# ant-nr-1
Accutase	StemcellTech	Cat# 07920
	Innovative Cell Technology	Cat# AT104-500
Y-27632	Stemgent	Cat# 04-0012
SB431542	Tocris	Cat# 1614
Doxycycline hyclate	Sigma	Cat# D9891
XAV939	Stemgent	Cat# 04-00046
LDN-193189	Stemgent	Cat# 04-0074
Zeocin	Invitrogen	Cat# 46-059
Glycine	Sigma	Cat# G7126
BDNF	R&D Systems	Cat# 248-BD/CF
GDNF	R&D Systems	Cat# 212-GD/CF
CNTF	R&D Systems	Cat# 257-NT/CF
Critical commercial assays		
RLTplus Lysis byffer	Qiagen	Cat# 1053393
RNeasy micro/mini plus kit	Qiagen	Cat# 74034
Deposited data		
Single cell RNA-seq (this study)	NCBI (dbGaP)	dbGaP Study Accession: phs002032.v1.p1
	Broad Institute Single Cell Portal	https://singlecell.broadinstitute.org/single_cell/study/SCP1972/berryer-tegtmeyer-et-al-hpsc-derived-astrocytes#study-summary
Experimental models: Cell lines		
WA01 ESC line (XY)	WiCell Research Institute	RRID:CVCL_9771
DS2U iPS line (XY)	WiCell Research Institute	RRID:CVCL_EJ82
DS1 iPS line (XY)	WiCell Research Institute	RRID:CVCL_EJ81
SCBB-1852 (XY)	Stanley Center Stem Cell Resource	Donor ID: ML832-2002
SCBB-1854 (XX)	Stanley Center Stem Cell Resource	Donor ID: ML832-6778
SCBB-1857 (XY)	Stanley Center Stem Cell Resource	Donor ID: ML611-3363
SCBB-1859 (XY)	Stanley Center Stem Cell Resource	Donor ID: ML611-2911
SCBB-1861 (XY)	Stanley Center Stem Cell Resource	Donor ID: ML787-4822

Continued

REAGENT or RESOURCE	SOURCE	IDENTIFIER
SCBB-1863 (XX)	Stanley Center Stem Cell Resource	Donor ID: ML844-6618
SCBB-1864 (XY)	Stanley Center Stem Cell Resource	Donor ID: ML898-3533
SCBB-1865 (XY)	Stanley Center Stem Cell Resource	Donor ID: ML898-5426
Human primary astrocytes	ScienCell	Cat# 1800
Software and algorithms		
ALPAQAS	CellProfiler	https://github.com/mberryer/ALPAQAS
MATLAB	MathWorks	https://github.com/lbinan/astrocyteInduction
Excel	Microsoft	https://www.microsoft.com
Prism 9.0	GraphPad Software	https://www.graphpad.com
R	The R Foundation for Statistical Study	https://www.r-project.org/foundation/

RESOURCE AVAILABILITY

Lead contact

Further information and any related requests for resources should be directed to and will be fulfilled by the lead contact, Dr. Nehme (rnehme@broadinstitute.org).

Materials availability

Engineered cell lines are available upon request to the corresponding authors and following appropriate institutional guidelines for their use and distribution. This study did not generate other unique reagents.

Data and code availability

- Bulk RNA-seq data are provided in Tables S1 and S5. Single cell RNA-seq data is publicly available via the NCBI (dbGaP Study Accession: phs002032.v1.p1) the Broad Institute Single Cell Portal (https://singlecell.broadinstitute.org/single_cell/study/SCP1972/berryer-tegtmeyer-et-al-hpsc-derived-astrocytes#study-summary). Other data are available in the manuscript or in the supplemental information and listed in the key resources table.

- All original code has been deposited at Github and is publicly available as of the date of publication.

- Any additional information is available from the lead contact upon request (rnehme@broadinstitute.org).

EXPERIMENTAL MODEL AND SUBJECT DETAILS

Cell culture

All studies using hPSCs followed institutional IRB and ESCRO guidelines approved by Harvard University. The human ESC line WA01 (H1, XY, RRID: CVCL_9771) and the human iPSC lines DS2U (XY, RRID: CVCL_EJ82) and DS1 (XY, RRID: CVCL_EJ81) were commercially obtained from WiCell Research Institute[47,48] (www.wicell.org). Additional human iPSC lines are from the Stanley Center Stem Cell Resource (https://sites.google.com/broadinstitute.org/sc-stem-cell-resource/) collection including SCBB-1852 (XY), SCBB-1854 (XX), SCBB-1857 (XY), SCBB-1859 (XY), SCBB-1861 (XY), SCBB-1863 (XX), SCBB-1864 (XY), SCBB-1865 (XY), and available from the NIMH Repository and Genomic Resource (NRGR). Each hPSC line was cultured in feeder-free conditions on Geltrex (ThermoFisher, Cat # A1413302, 15mg/mL) in StemFlex media (Gibco, Cat # A3349401) with 0.2% Normocin (Invivogen, Cat # ant-nr-1). For routine maintenance, cultured cells underwent daily medium changes and were passaged when reaching 70-80% confluence. Here, new 6-well NUNC plates (ThermoFisher Scientific, Cat # 140675) were coated with Geltrex for 1hr at 37°C. iPSC colonies were dissociated with Accutase (StemcellTech, Cat # 07920) for 5-10 min at 37°C. After incubation, cells were triturated to remove any excess cells from the plate bottom. Accutase-cell suspensions were added to mTeSR1 medium + 10μM Y-27632 (5 mM, Stemgent, Cat # 04-0012) in a 15mL Falcon tube. Cells were centrifuged at 300g, 5 min. The cell pellets were then resuspended in mTeSR1 medium + 10μM Y-27632 and plated across new plates at a desired split ratio (between 1:5 and 1:20). Cells were maintained in a humidified incubator at 37°C and 5% CO_2. hPSCs between passage 10 and 35 were used in this work.

Human induced astrocyte (hiA) generation

On day 0, hPSCs were differentiated in N2 medium [500 mL DMEM/F12 (1:1) (Gibco, Cat # 11320-033), 5 mL Glutamax (Gibco, Cat # 35050-061), 7.5 mL Sucrose (20%, SIGMA, Cat # S0389), 5 mL N2 supplement B (StemCell Technologies, Cat # 07156)] supplemented with SB431542 (10 µM, Tocris, Cat # 1614), XAV939 (2 µM, Stemgent, Cat # 04-00046) and LDN-193189 (100 nM, Stemgent, Cat # 04-0074) along with doxycycline hyclate (2 µg.mL^{-1}, Sigma, Cat # D9891) with Y27632 (5 mM, Stemgent, Cat # 04-0012). Day 1 was a step-down of small molecules, where N2 medium was supplemented with SB431542 (5 µM), XAV939 (1 µM) and LDN-193189 (50 nM) with doxycycline hyclate (2 µg.mL^{-1}) and Zeocin (1 µg.mL^{-1}, Invitrogen, Cat # 46-059). On day 2, N2 medium was supplemented with doxycycline hyclate (2 µg.mL^{-1}) and Zeocin (1 µg.mL^{-1}). Starting on day 2 human induced neural progenitor-like cells were harvested with Accutase (Innovative Cell Technology, Inc., Cat # AT104-500) and re-plated at 15,000 cells.cm^{-2} in Astrocyte Medium (ScienCell, Cat # 1801) with Y27632 (5 mM) on geltrex coated plates. Cells were maintained for > 30 days in Astrocyte Medium (ScienCell, Cat # 1801).

Human primary astrocytes (hpAs)

Human primary cortical astrocytes (hpA) were obtained from ScienCell Research Laboratories (ScienCell, Cat #1800) and cultured according to the manufacturer's instructions.

All cell lines were tested for mycoplasma contamination.

METHOD DETAILS

Immunocytochemistry

Immunofluorescence was performed using an automatic liquid handling dispenser (ApricotDesigns, Personal Pipettor). Cells were washed abundantly in 1x PBS, fixed for 20 minutes in PFA (4%, Electron Microscopy Sciences, 15714-S) plus Sucrose (4%, SIGMA, S0389), washed abundantly in 1x PBS, permeabilized and blocked for 20 minutes in Horse serum (4%, ThermoFisher, 16050114), Triton X-100 (0.3%, SIGMA, T9284) and Glycine (0.1M, SIGMA, G7126) in 1x PBS. Primary antibodies were then applied at 4°C overnight in 1x PBS supplemented with Horse serum (4%). The following primary antibodies were used: Rabbit anti-human Aquaporin 4 (1:100, Millipore, AB3594), Rat anti-human CD44 (1:500, ThermoFisher, 14-0441-82), Rabbit anti-human SLC1A3 (1:500, Boster, PA2185), Rabbit anti-human S100b (1:200, Abcam, ab52642, RRID:AB_882426) and Rabbit anti-human Vimentin (1:100, Cell Signaling, 3932S, RRID:AB_2288553).

TNFα stimulation

Human primary and induced astrocytes (> day 30 of differentiation) were seeded at 15,000 cells.cm^{-2} in 96-well plates and incubated 24 hours later with human Tumor Necrosis Factor alpha (Sigma Aldrich, H8916, 100ng.mL^{-1}) or 0.1% Bovine Serum Albumin (Sigma Aldrich, A0281-10G) in Astrocyte medium (ScienCell, 1800) for 7 days. The media was replaced with fresh treatment after 4 days of incubation. Media were collected and stored at -80°C until further processing. IL-6 concentration was measured by ELISA (Abcam, ab229334) in supernatants diluted 1:50 according to the manufacturer's protocol (Abcam).

hN generation and synapse quantification

Human induced neuron (hN) generation, astrocyte co-culture and synapse quantification was performed as previously described.[15,30,49] In brief, hNs with stable integration of iNGN2 in the AAVS1 safe-harbor locus were differentiated on day 0 in N2 medium supplemented with SB431542, XAV939 and LDN-193189 along with doxycycline and Y27632. On day 1, N2 medium was supplemented with SB431542, XAV939 and LDN-193189 along with doxycycline and Zeocin. On day 2, N2 medium was supplemented with doxycycline and Zeocin. Starting on day 3, cells were maintained in Neurobasal media (NBM) supplemented with B27, BDNF, CTNF, GDNF (10 ng.mL-1, R&D Systems 248-BD/CF, 257-NT/CF and 212-GD/CF) and doxycycline. On days 4 and 5, NBM was complemented with floxuridine. On day 6, hNs and hpAs were harvested with Accutase, and plated in NBM using a liquid handling dispenser (Personal Pipetter, ApricotDesigns) in the 60-inner wells of geltrex-coated 96-well plates. Co-cultures were then maintained in NBM until fixation and immunostaining on day 21 of hN differentiation. Immunofluorescence was performed using an automatic liquid handling dispenser (Personal Pipetter, ApricotDesigns) using Rabbit anti-human SYNAPSIN1 (1:1000, Millipore, AB1543, RRID:AB_2200400) and Chicken anti-human MAP2 (1:1000, Abcam, ab5392, RRID:AB_2138153) primary antibodies, Goat anti-chicken AlexaFluor 488 (1:1000, ThermoFisher, A21131), Donkey anti-rabbit AlexaFluor 555 (1:1000, ThermoFisher, A31572) secondary antibodies, as

well as DAPI (1:5000, ThermoFisher Scientific, D1306) and TrueBlack (1:5000, Biotium, 23007). Images were acquired with a high-content screening confocal microscope (Opera Phenix, PerkinElmer, RRID:SCR_021100), analyzed with CellProfiler pipelines (https://github.com/mberryer/ALPAQAS).

Calcium imaging and analysis

Cells were incubated in fura-4AM dye at 2μM for 30 min at 37C. Cells were then washed and imaged in 200 μL recording solution (125mM NaCl, 2.5mM KCl, 15mM HEPES, 30mM glucose, 1mM $MgCl_2$, 3mM $CaCl_2$ in water, pH 7.3, mOsm 305). Time lapse videos were acquired at 4X on a Nikon Ti2-E microscope at 2 Hz for 5 mins. Cells were stimulated after 1 min by addition of 200 μL of ATP at 500μM in recording solution, generating a final concentration of 250 μM in the well. Analysis of calcium videos was done using a custom MATLAB script. First, cells were segmented using a watershed algorithm. A table of mean fluorescence per cell across time was generated. Traces were smoothed with a Savitzky-Golay filter with a span of 50 images, aligned on the X-axis by subtracting the minimal value, then the peaks of a minimum height and local prominence of 10, with a minimal distance of 3 seconds between peaks were detected. We then extracted features for each cell: the number of peaks, peak height, interval and duration, rising time and falling time (defined as the time between the peak and the previous/next change of sign in the derivative). Data from all samples (4 wells of primary cells, and 8 wells of induced astrocytes from 2 parental cells, 4 wells each) were Z-scored then pooled together before k-means clustering with k=5. Data were then re-split into 12 tables according to the origin of each cell for statistics. For each cluster, example traces for 60 cells randomly picked from all 12 samples of origin were generated by normalizing all traces between 0 and 255 and generating an 8-bit image (Figure S2). Scripts are available here https://github.com/lbinan/astrocyteInduction.

3′ DGE bulk mRNA-sequencing and analysis of hPSCs, hiAs and hpAs

Four to five biological replicates per cell type of human pluripotent stem cells, human primary cortical astrocytes, and human induced astrocytes (>day 30 of differentiation) were harvested in RLTplus Lysis buffer (Qiagen, 1053393). Total RNA was isolated using the RNeasy micro/mini plus kit (Qiagen, 74034) and stored at -80°C. Total RNA was quantified using the Qubit 2.0 fluorometric Assay (Thermo Fisher Scientific). Libraries were prepared from 125 ng of total RNA using a 3′DGE mRNA-seq research grade sequencing service (Next Generation Diagnostic srl)[50] which included library preparation, quality assessment and sequencing on a NovaSeq 6000 sequencing system using a single-end, 100 cycle strategy (Illumina Inc.). The raw data were analyzed by Next Generation Diagnostics srl proprietary 3′DGE mRNA-seq pipeline (v1.0) which involves a cleaning step by quality filtering and trimming, alignment to the reference genome and counting by gene.[51,52] Differential expression analysis was performed using edgeR.[53] Samples were sequenced and analyzed at TIGEM (Pozzuoli, Italy).

Bulk mRNA-sequencing and analysis of DS1 and DS2U hiAs

Two biological replicates of DS1 and two biological replicates DS2U hiAs were harvested in RLTplus Lysis buffer (Qiagen, 1053393). Total RNA was isolated using the RNeasy micro/mini plus kit (Qiagen, 74034). Libraries were prepared using Roche Kapa mRNA HyperPrep strand specific sample preparation kits from 200ng of purified total RNA according to the manufacturer's protocol using a Beckman Coulter Biomek i7. The finished dsDNA libraries were quantified by Qubit fluorometer and Agilent TapeStation 4200. Uniquely dual indexed libraries were pooled in equimolar ratio and subjected to shallow sequencing on an Illumina MiSeq to evaluate library quality and pooling balance. The final pool was sequenced on an Illumina NovaSeq 6000 targeting 30 million 100bp read pairs per library. Sequenced reads were aligned to the UCSC hg19 reference genome assembly and gene counts were quantified using STAR (v2.7.3a).[52] Differential gene expression testing was performed by DESeq2 (v1.22.1).[54] RNAseq analysis was performed using the VIPER snakemake pipeline.[55] Library preparation, Illumina sequencing and VIPER workflow were performed by the Dana-Farber Cancer Institute Molecular Biology Core Facilities. Gene Ontology (GO) analysis of differentially expressed genes was performed using Metascape.[56]

scRNA-sequencing and donor assignment

For single-cell analyses, cells were harvested and prepared with 10X Chromium Single Cell 3′ Reagents V3 and sequenced on a NovaSeq 6000 (Illumina) using a S2 flow cell at 2 x 100bp. Raw sequence files were then aligned and prepared following the Drop-seq workflow.[57] Human reads were aligned to GRCh18 and filtered for high quality mapped reads (MQ 10). In order to identify donor identity of each droplet, variants

were filtered through several quality controls as described previously to be included in the VCF files,[25] with the goal of only using sites that unambiguously and unequivocally can be detected as A/T or G/C. Once both the sequenced single-cell libraries and VCF reference files are filtered and QC'ed, the Dropulation algorithm is run. Dropulation analyzes each droplet, or cell, independently and for each cell generates a number representing the likely provenance of each droplet from one donor. Each variant site is assigned a probability score for a given allele in the sequenced unique molecular identifier (UMI) calculated as the probability of the base observed compared to expected based, and 1 – probability that those reads disagree with the base sequenced. Donor identity is then assigned as the computed diploid likelihood at each UMI summed up across all sites.[25]

scRNAseq analysis of villages and integrated datasets

Gene by cell matrices from hiA villages were built from separate runs of 10X Chromium Single Cell 3′ Reagents V3 as described above. Cells with less than 200 genes and more than 15% mitochondrial RNA were trimmed away from downstream analyses. SNN graphs were computed using batch-balanced k-nearest neighbors (BBKNN) to remove batch effects across 10X reactions.[58] Leiden clustering was performed across resolutions in BBKNN space (0.2,0.4,0.6) and then visualized to determine the dimensionality of the data. LEIDEN_BBKNN_0.2 was used for the downstream analysis. For the metagene analysis, summed expression of gene sets for astrocyte precursor markers and mature astrocyte markers were divided by a random control set of 500 genes. For the analyses where we integrated existing iPSC-astrocyte data as well as human brain data, raw matrices were loaded in Seurat v4.0.1. The same parameters were applied as above, excluding cells with fewer than 200 genes and greater than 15% mitochondrial gene expression. Given the technical variability across datasets, and cell sources, we first computed a new count matrix using SCTransform.[59] Next, the transformed data was integrated using linked inference of genomic experimental relationships (LIGER).[60] Downstream analytical steps were performed using Seurat v4.0.1 basic functions. The *in vitro* datasets which were used for comparison are as follows; Leng et al, 2022[28] are under GEO accession GSE182308 using vehicle control sample GSM5526488; Barbar at al, 2020[29] CD49 positive astrocytes found at https://www.synapse.org/#!Synapse:syn21861229, using CD49 positive sample 51121CD49fpos; Rapino et al, 2022,[27] hiAs from https://singlecell.broadinstitute.org/single_cell/study/SCP1960/hpsc-derived-astrocytes-from-rapino-et-al-2022, using sample 1016A_astrocytes_rep1_A1.auto.10X.exonic+intronic.digital_expression.txt.

QUANTIFICATION AND STATISTICAL ANALYSIS

CellProfiler, calcium imaging, bulk and scRNAseq data were compiled with Microsoft Excel and analyzed using Prism 9.0 (GraphPad Software) or R (The R Foundation for Statistical Study). Bar graphs are shown as mean +/- SEM, unless otherwise specified, and specific statistical tests and the exact value of n are identified in the legends. Significance was determined with a p-value <0.05 (* $p<0.05$, ** $p<0.01$, *** $p<0.001$). No statistical methods were used to predetermine the sample size. Data collection was not randomized and data analysis was not performed blind to the experimental condition.